Aerodynamic Roll Control on Project Xanthus

Connor Sterling

November 2025

1 Introduction

Project Xanthus was the MIT Rocket Team's demonstrator launch vehicle designed to test a number of critical subsystems on Project Zephyrus, most notably active roll control. Xanthus was launched twice in November, 2025 at URRG. In the first flight, roll control was not established. In the second flight, roll control was established but failed to achieve asymptotic stability.

This report provides a comprehensive description of the control system design process, performance, and evaluation. Section 2 briefly explains the system dynamics. Section 3 details control system design. Section 4 recounts the events at launch. Telemetry data are analyzed in Section 5. Section 6 concludes the report.

2 Roll Dynamics

The governing equation for a rocket in roll is

$$J_{xx}\ddot{\phi} + C\dot{\phi} = M_x. \tag{1}$$

Here, J_{xx} is the moment of inertia in x, C is (linearized) aerodynamic damping, and M_x is the net moment about the roll axis. The roll angle is designated as ϕ.

Xanthus uses aileron-like control surfaces ("tabs") located at the back of two fins. They are actuated by servo motors. Fig. 1 shows the Xanthus fin can. The left fin is "Dusty Doughnut", the right "Crusty Cranberry". Centered is "Trusty Turnip", and behind the rocket is "Rusty Radish". The tabs are painted orange. They are limited in motion to $\pm 10°$, as this is the range over which the linearization of the aerodynamics is expected to hold.

The moment due to forces on the tab is given in terms of tab angle of attack α as

$$M_x = M_x^{aero} = \frac{1}{2}\rho V^2 S R C_{L\alpha} N_{tabs} \alpha, \tag{2}$$

Figure 1: Xanthus fin can, as seen on the launch rail. Tabs are painted orange. Left: "Dusty Doughnut". Center: "Trusty Turnip". Right: "Crusty Cranberry". Not pictured: "Rusty Radish".

where ρ and V are air density and speed, S is the tab area and R is the effective lever arm, and $C_{L\alpha}$ is the derivative of the lift coefficient with respect to α. We define $\frac{\partial M_x}{\partial \alpha}$ as G_α, "aerodynamic gain." The roll transfer function can then be written as

$$\frac{\phi}{\alpha} \equiv G = \frac{G_\alpha}{J_{xx}s^2 + Cs}. \tag{3}$$

The dynamics of the servo motor are of the form

$$\frac{\alpha}{\alpha^*} = G_{servo}^{CL} = \frac{b_2 s^2 + b_1 s + b_0}{a_3 s^3 + a_2 s^2 + a_1 s + a_0}. \tag{4}$$

A star indicates commanded value. For a controller K, the full system closed loop transfer function is

$$\frac{\phi}{\phi^*} = \frac{K \cdot G_{servo}^{CL} \cdot G}{1 + K \cdot G_{servo}^{CL} \cdot G}. \tag{5}$$

The full block diagram is pictured in Fig. 2. Measurement devices H are approximated as unity. Dashed lines indicate digital computers. The complex inner loop α/α^* is condensed into G_{servo}^{CL}.

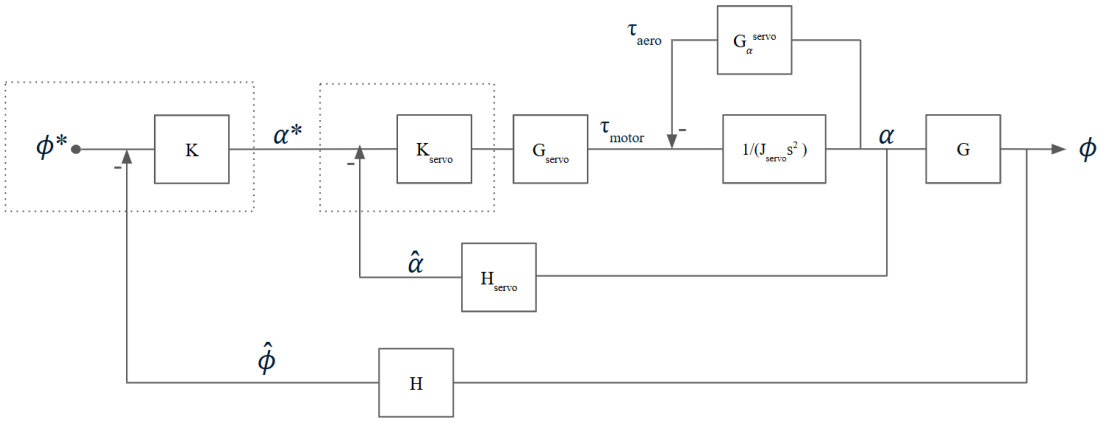

Figure 2: Roll dynamics block diagram. Dynamics are denoted by G, controllers K, and measurement devices H. A star indicates commanded value, a circumflex indicates estimated value. Dashed boxes signify digital computers.

A more in-depth discussion of roll and servo dynamics can be found in [1]. For the determination of the coefficients a_i and b_i in the servo transfer function, see [2]. Information on Xanthus' design can be found at [3].

3 Controller Design

The design of Xanthus' controller was accomplished through classical root locus and frequency methods. The controller takes the form of a PID controller:

$$K = K_p + K_d s + \frac{K_i}{s} \tag{6}$$

The aerodynamic damping C was determined to be negligible [4]. For $C \approx 0$, the open loop system has two free integrators. This all but precludes the use of an integrator, as phase at zero frequency is nearly -180°. The use of an integrator is unnecessary anyway, as for the idealized system (with $C = 0$) steady state error in step and ramp tracking is zero. Considering the existence of roll-moment inducing manufacturing defects, it can be shown that the steady state error e_{ss} will asymptote a small value:

$$e_{ss} = \frac{M_x^{ss}(q)}{G_\alpha(q) K_p}. \tag{7}$$

In the above, $M_x^{ss}(q)$ represents the "steady state" moment due to manufacturing defects or asymmetries as a function of dynamic pressure. Note that the error is directly proportional to dynamic pressure, a time dependent quantity for a rocket flight. Thus, the term "steady state" is used loosely. Since the primary objective of controlling roll is to prevent the rocket from spinning, constant error to step inputs is inconsequential. K_i is therefore set to zero and the controller takes the form

$$K = K_p(T_d s + 1). \tag{8}$$

Note that the transfer function ϕ/ϕ^* is not time invariant. Both aerodynamic and physical properties change throughout the course of the flight. Moment of inertia will decrease as propellant is expelled. Air density changes with altitude. Most importantly, the velocity varies immensely across the flight. For Xanthus, this range is predicted as ranging from 0 to 120 m/s. The dynamic pressure, $q = \frac{1}{2}\rho V^2$ is highly influential on the aerodynamic gain. Thus, a controller that functions at 100 m/s will not perform the same at a flight speed of 80 m/s.

To surmount this difficulty it is necessary to design a time-varying controller with gains dependent on dynamic pressure and moment of inertia. For Xanthus, reduction in J_{xx} is neglected. The controller then takes the form

$$K(t) = K_0 \cdot \frac{q_0}{q(t)}, \tag{9}$$

where K_0 is a controller designed at reference dynamic pressure q_0. A reference velocity of 100 m/s was chosen for the Xanthus controller design and air density was assumed constant. Choice of reference dynamic pressure has no effect on the control design for the low speed regimes considered.

The choice of K_p and T_d sought to make the dominant system poles as fast as possible while maintaining adequate damping and stability margins. This resulted in $K_p = 0.1887$ and $T_d = 0.20$ s. Figs. 3 and 4 display the root locus and Bode plots for the system. In Fig. 3, the design closed loop poles are marked in red. In Fig. 4, crossover frequencies are marked by dashed lines to illustrate the stability margins.

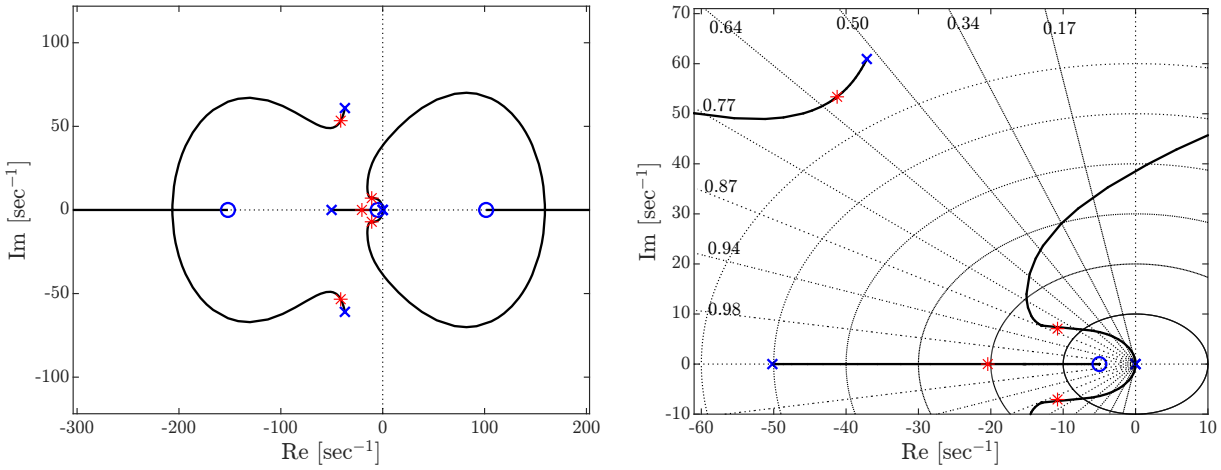

(a) **(b)**

Figure 3: Root locus plot indicating chosen poles as red stars. The two open loop poles at (or approximately at) the origin are the rigid body roll dynamics. The left and right zeros and all other poles are from the servo dynamics. The center zero is due to the controller.

For this design, gain crossover occurs at 2.05 Hz. Phase margin is 41.01°. Phase crossover occurs at 6.14 Hz. Gain margin is 3.27. The greatest uncertainties in the model lie in values that scale the transfer function (J_{xx}, G_α). I.e. error in modeling these quantities will change the effective gain of the system, moving the closed loop poles along the root locus toward instability for underestimations. For this reason, gain margin is the most important stability metric to consider. Saturation effects from the tab's limited range of motion are neglected, as they will generally be benign from a stability perspective.

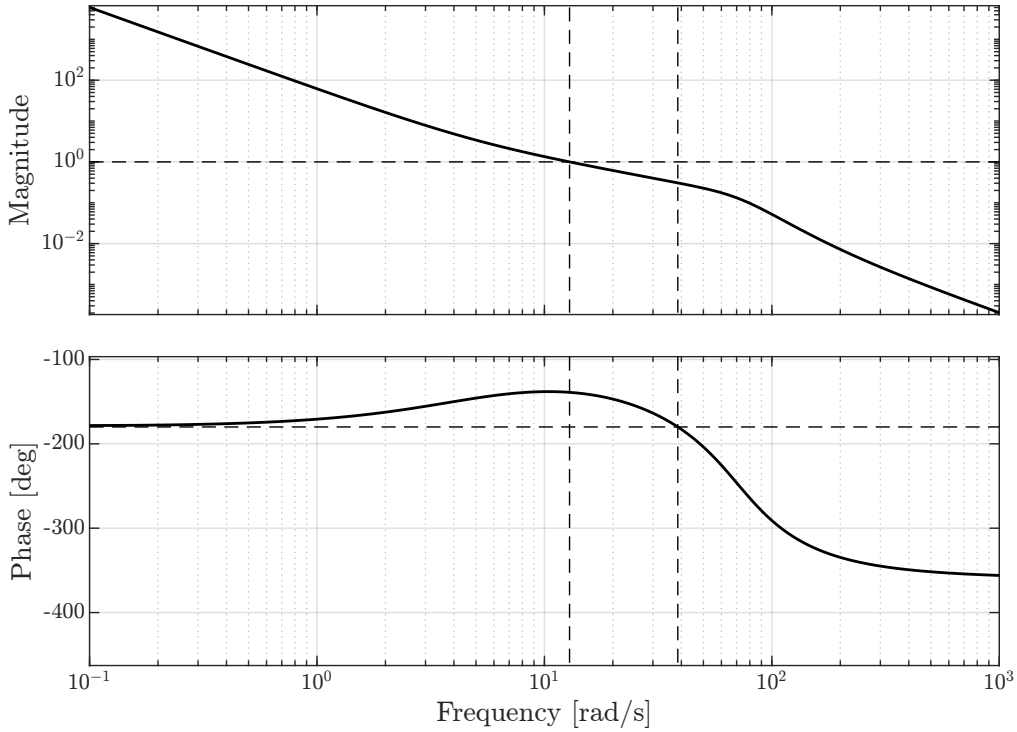

Figure 4: Bode plot indicating crossover frequencies and margins. Gain margin is 3.27 with $|L| = 1$ at 2.05 Hz. Phase margin is 41.01° with $\angle L = -180°$ at 6.14 Hz.

4 Launch Summary

Xanthus was launched for the first time on November 8th, 2025 at approximately 9:30 a.m. at the Upstate Research Rocketry Group facility in Penn Yan, NY. According to accelerometer data, it achieved an apogee of 381 m (1,251 ft). Maximum flight speed was 86 m/s (282 ft/s). Figure 5 displays the flight profile.

There was a bug in the accelerometer data processing code that resulted in anomalous velocity readings. Integration of the accelerometer was paused during preflight mode, beginning after launch detection. However, the initial time step is calculated using the time before entering preflight mode and the time at launch detection. This huge Δt is multiplied by the accelerometer reading in an integration calculation to get velocity, yielding an initial airspeed of over 25,000 m/s. Recall Eq. 9. The square of velocity appears in the denominator of $K(t)$. Because Xanthus believed it was traveling at above Mach 50, $K(t) = 0$ for the duration of the flight and the tabs did not actuate. Consequently, the rocket rolled uncontrollably.

The recovery system deployed successfully. (One novelty of Xanthus is the use of a reefing parachute. This is of little interest from a control perspective, though.) Upon deployment, high decelerations caused the motor retention system to fail, causing it to slide partially out from the bottom of the rocket. When Xanthus struck the ground, the motor acted as a lever, transmitting stresses of above 240 MPa into the aluminum bulkhead used to align the motor. The latter was plastically deformed and rendered non-functional. Moreover, the tab on "Crusty Cranberry" was damaged, limiting its range of motion to one direction.

There was no replacement bulkhead, and without a way to mount a second motor aligned axially Xanthus could not fly again. This engineer and the Aerodynamics and Control teamlead spent an hour flattening the bulkhead with a sledgehammer and pliers until it was flightworthy. They also restored functionality to "Crusty Cranberry", though it is unclear as to whether or not the tab performed at its preflight levels.

Xanthus' second launch occurred at roughly 4:00 p.m. on the same day. Apogee was at 398 m (1305 ft), maximum speed was 89 m/s (292 ft/s). The flight profile is shown in Fig. 6. The bug in velocity calculation had not been discovered, and so a controller independent of dynamic pressure was required. In an effort to maintain authority across the anticipated flight velocities, this engineer elected to increase K_p to 0.5284 while maintaining T_d.

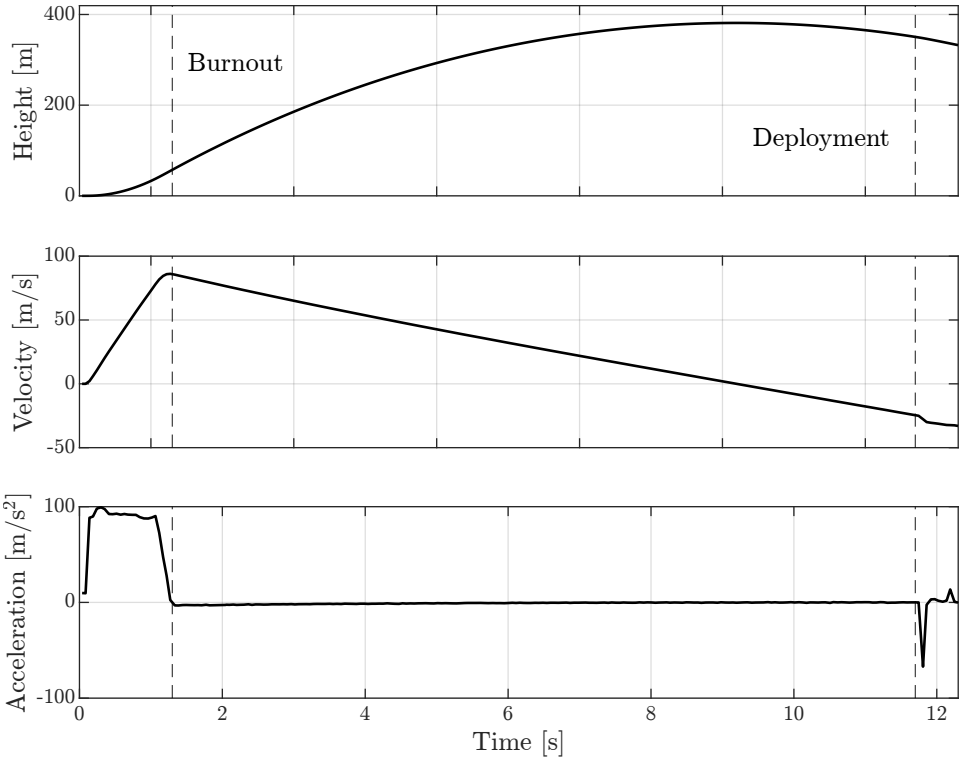

Figure 5: Flight I profile until deployment. Max height: 381 m. Max velocity: 86 m/s.

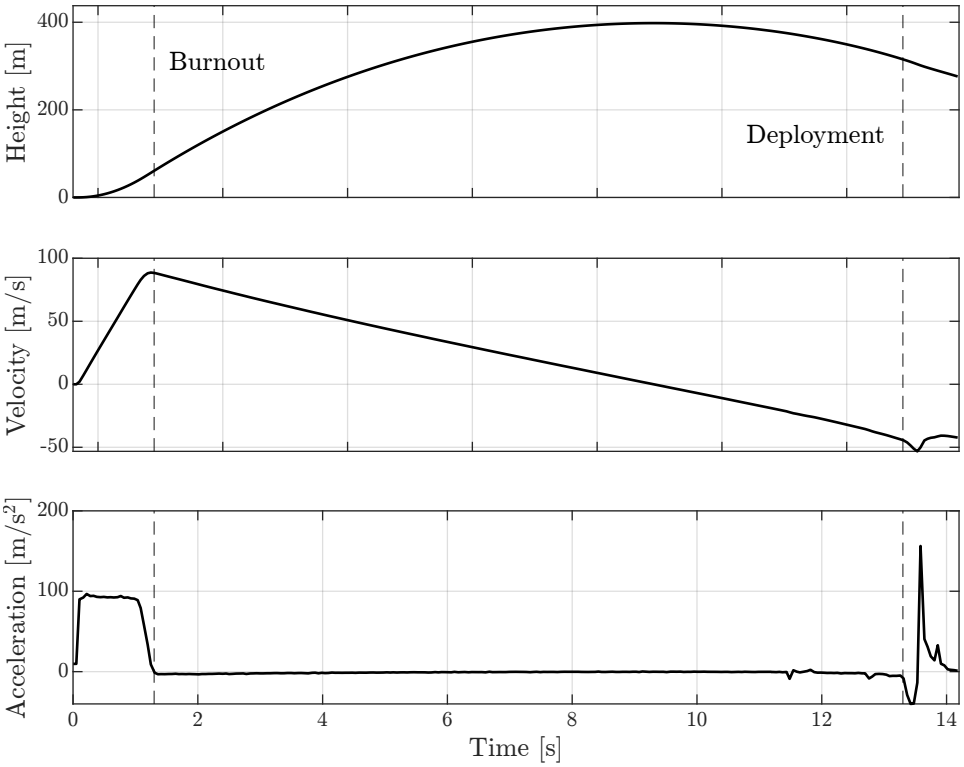

Figure 6: Flight II profile until deployment. Max height: 398 m. Max velocity: 89 m/s.

Without reliance on velocity data, roll control was successfully established. However, the system exhibited instability, with oscillations in roll angle growing exponentially until the tab angle saturated at ±10°. This was the result of a second bug, in which the angular velocity was converted to rad/s for no reason. The controller was therefore implemented as

$$K = K_p + K_d \cdot \frac{\pi}{180} s. \tag{10}$$

The issue with this is obvious by inspection. Multiplying K_d by $\pi/180$ effectively reduces it to negligibility. The consequences of this are further explored in the following section, as are the implications for future control design. Parachute deployment and recovery was successful.

Ultimately, Xanthus' launch can be characterized as a partial success overall and in terms of control. It marks the first time MIT Rocket Team launched the same vehicle twice in one day with two successful recoveries. It also marks the first time the team achieved active control over the roll DOF. That being said, stability in roll was not achieved.

5 Analysis

Despite the lack of roll stabilization, Xanthus' flights can still provide valuable insight into the fidelity of our modeling. From flight two, we can gauge the error in our system modeling by comparing theoretical and observed responses to the defective controller.

Fig. 7 displays roll angle ϕ, tab angle command α^*, and dynamic pressure normalized by the design dynamic pressure, q/q_0. The onset of instability was immediate, with roll oscillation amplitude growing until about two seconds. At this point, the tab command angle begins to saturate, and the roll angle enters a limit cycle.

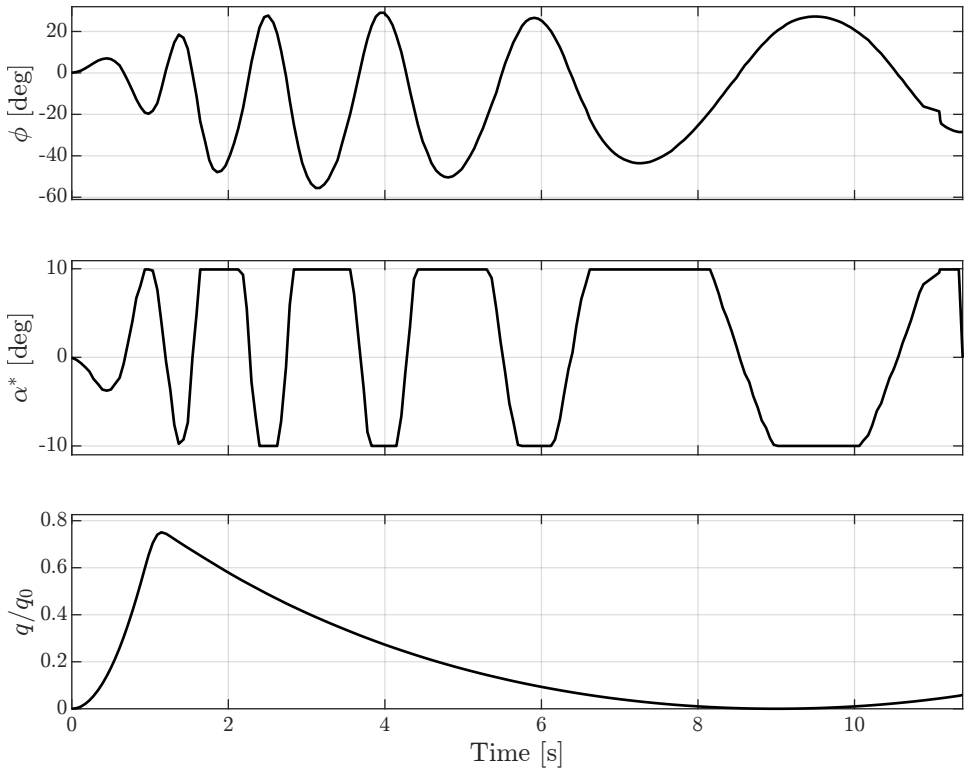

Figure 7: Roll angle, commanded tab angle, and normalized dynamic pressure on flight II. Oscillation amplitude in ϕ increases until about three seconds, where saturation effects arrest the growth of instability. Frequency decreases as q drops.

The most informative aspect of the flight is the changing frequency of oscillation. The natural frequency of the system is equal to the distance of the dominant poles from the origin (under a dominant pole approximation). For the time varying controller described in section 3, the location of the dominant poles does not change because K is adjusted based on dynamic pressure. However, for the time-invariant controller implemented for Xanthus' second flight the dominant pole location will change with dynamic pressure. Recall that the choice of $K = 0.5284 \cdot ((0.2\text{sec})s + 1))$ was intended to ensure the dominant poles would provide acceptable performance for all expected dynamic pressures. As noted in Eq. 10, the actual implemented controller was

$$K = 0.5284 \cdot \left((0.2 \text{ sec}) \ s \cdot \frac{\pi}{180} + 1\right) \approx 0.5284. \tag{11}$$

After burnout moment of inertia is constant. Neglecting aerodynamic damping, the dominant pole location is a function exclusively of two quantities: dynamic pressure and "effective gain", k_{eff}. Because the tab angle saturates, the controller gain K_p that the system experiences is a fraction of the unsaturated gain. Effective gain is defined as

$$k_{\text{eff}} = \frac{K}{K_{\text{unsat}}} = \frac{\alpha^*}{\alpha^*_{\text{unsat}}}. \tag{12}$$

It is the ratio of actual (nonlinear, saturated) tab command angle to theoretical (linear, unsaturated) tab command angle. Fig. 8 compares α^* and α^*_{unsat}. By definition, $k_{\text{eff}} = 1$ except when the tab command saturates (i.e. $|\alpha^*_{\text{unsat}}| > 10°$).

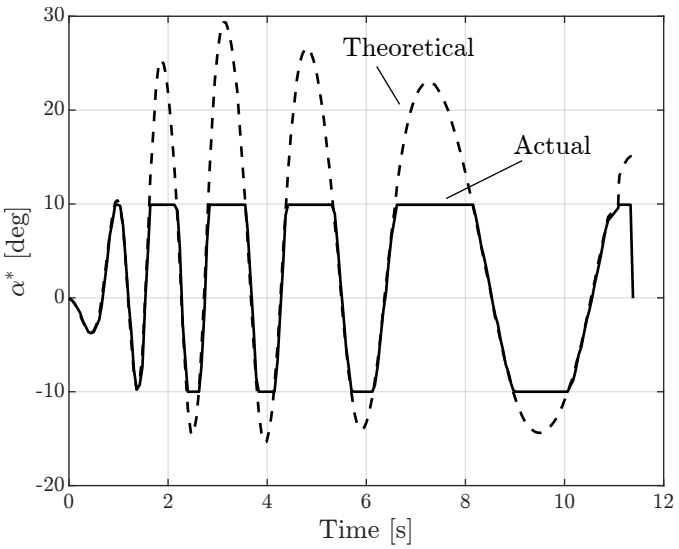

Figure 8: Comparison of actual, saturated tab command angle to unsaturated theoretical command.

The open loop transfer function at any time t can thus be written as

$$L = K \cdot G_{servo} \cdot G_q \cdot q \cdot k_{\text{eff}}, \tag{13}$$

where G_q is $\frac{\partial G}{\partial q}$, which is constant with respect to q. The closed loop poles are the roots of $1 + L$. For any instant, the natural frequency of the system is roughly the frequency of the dominant poles at that time. In this case, the dominant poles are the roots of $1 + L$ with positive real parts. While we cannot measure the instantaneous natural frequency of the system, an average, $\overline{\omega}_n$, can be estimated as

$$\overline{\omega}_n = \frac{2\pi}{\Delta t_{pk}}, \tag{14}$$

where Δt_{pk} is the time between peaks of the roll angle response. From Eq. 13, we can predict $\overline{\omega}_n$ for a given peak-to-peak time interval by computing an average open loop transfer function, $\overline{L}$ over the interval

and finding the roots of $1 + \overline{L}$. Effectively,

$$\overline{L} = \frac{1}{t_{pk,2} - t_{pk,1}} \int_{t_{pk,1}}^{t_{pk,2}} K \cdot G_{servo} \cdot G_q \cdot q(t) \cdot k_{\text{eff}}(t) dt. \tag{15}$$

A comparison of natural frequency as measured according to Eq. 14 to that predicted via Eq. 15 is presented in Fig. 9. Natural frequencies are plotted at the center of the time interval over which they are computed. As expected, natural frequency declines with the product $k_{\text{eff}}(t) \cdot q(t)$. The theoretical model consistently overpredicts the observed natural frequency. The final data point is considered too close to apogee to be reliable (the assumption that the rocket is traveling straight up may not be valid) and is neglected in the analysis. Interestingly, the discrepancy between observation and prediction appears to be greater after large saturation events. Since k_{eff} is considered in the calculation, this may be the result of higher order or nonlinear hysteresis effects. It could also be coincidence.

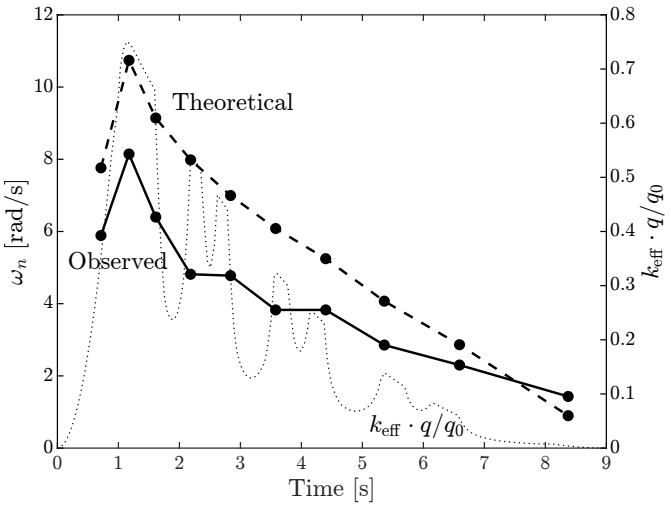

Figure 9: Comparison of theoretical and observed mean natural frequencies against the time-varying component of L, $k_{\text{eff}}(t) \cdot q(t)$. Mean natural frequency is overpredicted.

Almost any aspect of the system model could be incorrect. The servo motor transfer function could be wrong, aerodynamic damping could be non-negligible, or air density could have been different than expected. However, we have high confidence in the servo model, particularly the pole and zero locations. The sensitivity of the model to damping or density variation is small enough that the range over which these quantities may differ from expected does not result in a significant error. The primary cause of error is instead anticipated to be incorrect prediction of G_α and J_{xx}. Recall Eq. 3. For negligible C, the ratio of these two terms will appear directly in the full open loop transfer function L. As this ratio changes, the closed loop poles will move along the root locus, changing the natural frequency. Fig. 10 depicts the position of the observed mean closed loop poles—i.e. the closed loop pole associated with each $\overline{\omega}_n$, assuming correct pole and zero locations.

The closed loop pole location on the root locus directly corresponds to the loop gain L. Comparing observed and theoretical values of L yields a metric for error:

$$\text{Error} = \frac{|L_{obs.}| - |L_{theor.}|}{|L_{theor.}|} \tag{16}$$

Across the nine considered half periods, the mean error was -50.1% with standard deviation 9.4%. This means that predicted loop gain was on average *twice* what occurred during flight. The methods used to calculate this statistic are estimations at best, but such a large difference indicates significant modeling error.

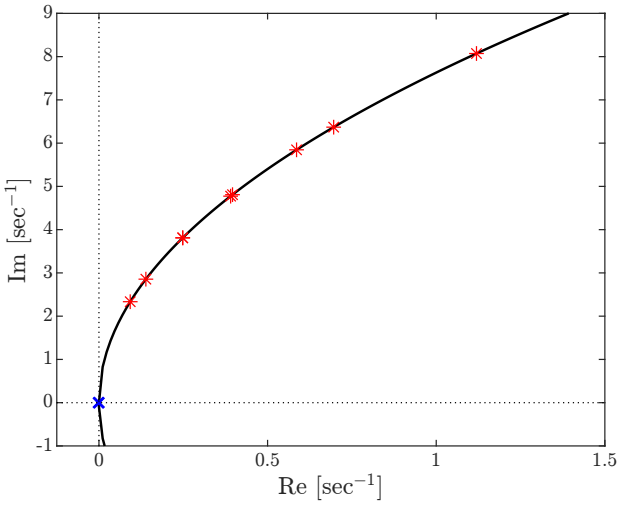

Figure 10: Observed mean dominant pole locations over each half period. Each mean natural frequency is mapped to a position on the root locus a distance $\overline{\omega}_n$ from the origin. From this position is derived the ratio $|\boldsymbol{L_{obs.}}|/|\boldsymbol{L_{theor.}}|$.

6 Conclusion

Why did Xanthus perform so differently than expected? Was the moment of inertia significantly underestimated? Do the tabs produce half the moment predicted by analytic results and CFD? Could this be due to simulation error or manufacturing defects? It is beyond the scope of this report to suggest a definitive explanation for the large prediction error.

The goal of Project Xanthus was to demonstrate active roll control and stabilization using tabs to justify the deployment of this technology on Project Zephyrus. Xanthus successfully demonstrated roll control on her second flight. Had it not been for the flawed implementation of the controller, analysis indicates that stabilization would have been achieved.

A number of challenges remain if active roll control is to be implemented on Project Zephyrus:

1. **Refinement of aerodynamic modeling.** An understanding of why Xanthus' flight differed so much from expectation is necessary for designing a controller to optimize performance. Without an accurate prediction of the aerodynamics and physical properties of a rocket, stabilization can still be achieved, but not necessarily in the best manner possible. Wind tunnel testing is the clear next step to solve this issue.

2. **Flight condition estimation.** Due to avionics issues a time-varying controller was not deployed on Xanthus. Because Zephyrus will experience an immensely broad range of flight conditions, this is critical to stabilizing roll over the entire flight. A reliable way of estimating the current moment of inertia, air density, and speed is essential. This will likely require a combination of accelerometer and barometer readings with predictions of propellant consumption.

3. **Moment of inertia estimation.** For Xanthus, a low confidence estimate of the roll moment of inertia was calculated using a SolidWorks assembly. Experimental validation of this estimate would be a prudent step to take for Project Zephyrus, since error in J_{xx} has a major impact on L.

4. **High speed control.** It is likely that different controllers will be required for subsonic, transonic, and supersonic regimes, as well as a way of switching between controllers when appropriate. In particular, the transonic regime presents a challenge due to high sensitivity of the aerodynamics (e.g. shock location and strength) to speed.

Although the scope and scale of these challenges are nontrivial, this engineer has confidence in the Aerodynamics and Control subteam to overcome them and establish active roll control *and* stabilization on Project Zephyrus. Time will tell if his faith is justified.

References

[1] O. Garcia, C. Casebolt, and C. Sterling, "Un-named Controls Project," 2025.

[2] C. Sterling, "Servo Motor Characterization for Project Xanthus," 2025.

[3] C. Casebolt *et al.*, "Project Zephyrus: Demonstrator Rocket Critical Design Review," 2025.

[4] S. Niskanen, "OpenRocket technical documentation," 2013.